

# Open Quantum Dynamics Calculations with the Hierarchy Equations of Motion on Parallel Computers

Johan Strümpfer<sup>†</sup> and Klaus Schulten\*,<sup>†</sup>,<sup>‡</sup>

**ABSTRACT:** Calculating the evolution of an open quantum system—i.e., a system in contact with a thermal environment—has presented a theoretical and computational challenge for many years. With the advent of supercomputers containing large amounts of memory and many processors, the computational challenge posed by the previously intractable theoretical models can now be addressed. The hierarchy equations of motion present one such model and offer a powerful method that has remained underutilized so far, because of its considerable computational expense. By exploiting concurrent processing on parallel computers, the hierarchy equations of motion can be applied to biological-scale systems. Herein, we introduce the quantum dynamics software *PHI* that solves the hierarchical equations of motion. We describe the integrator employed by *PHI* and demonstrate *PHI's* scaling and efficiency running on large parallel computers by applying the software to the calculation of intercomplex excitation transfer between the light-harvesting complexes 1 (LH1) and 2 (LH2) of purple photosynthetic bacteria, which involves a 50-pigment system.

# 1. INTRODUCTION

Quantum dynamics plays a major role in many biological processes.<sup>1–4</sup> To model such processes, one must account for the environment in which they occur, that is, one where thermal noise at an ambient temperature is present. Although many methods have been developed that account, to some degree, for the interaction between a quantum system and a thermal environment, <sup>4–16</sup> they typically involve limitations, with regard to the relative interaction strengths found within a system and between the system and environment, or make approximations regarding the quantum nature of the system, or neglect non-Markovian effects. Such limitations and approximations are often permissible for a particular system and then the respective methods yield valuable insight, but they generally do not apply.

Purple bacteria are one of the simplest photosynthetic life forms, capable, through efficient light harvesting, of living in photon-poor environments.<sup>17</sup> The primary pigment-protein complexes found in purple bacteria, light-harvesting complex 2 (LH2), light-harvesting complex 1 (LH1), and the reaction center (RC), have evolved to rapidly transfer excitation energy across many tens of nanometers and convert it, before the energy is lost through fluorescence or internal conversion, to a more stable form, resulting in a light-harvesting efficiency of >90%.  $^{18,19}$ This remarkable efficiency due to rapid excitation transfer has been the subject of many experimental 20-29 and theoretical 30-37 investigations. It has been shown that excitation transfer benefits not only from quantum coherence, 38-40 but also from environmental noise.  $^{40-47}$  In order to model excitation dynamics in purple bacteria, one must take into account the strong interactions not only between the excited states themselves, but also with their surrounding environment. 34,48-54

There are only a few quantum dynamics methods for computation of open quantum system density matrices that take into account arbitrary intrasystem and system—environment interactions, include non-Markovian effects, and make no assumptions about the quantum nature of the dynamics.<sup>55–61</sup> The hierarchy equations of motion (HEOM) of Tanimura and Kubo, <sup>58</sup> which employ a hierarchy of auxiliary density matrices to account for non-Markovian dynamics without resorting to perturbative approximations, 58-71 is one of the earliest open quantum system descriptions and remains the only one applicable to large systems. 34–36,71 Although the HEOM are computationally expensive, typically requiring many gigabytes (GBs) of computer memory and many days of computation time, their application to large systems has been possible by exploiting  ${\rm GPUs}^{72}$  and highly parallel computers.  $^{34-36}$  The GPU-HEOM implementation<sup>72</sup> yields tremendous improvement in the computation time, but is severely limited to small (<10 pigments) systems by the small amount of memory available with current-generation GPUs. By performing the HEOM integration on multiprocessor CPUs, the system size is limited by the much-larger main computer memory instead of GPU memory, allowing much larger systems to be modeled, as shown here.

However, implementing the HEOM on a multiprocessor computer is difficult, because of the highly connected nature of the auxiliary density matrices. To achieve peak performance, the communication between processing elements must be minimized through a partitioning scheme that assigns each matrix in the hierarchy to a different processor. Additional improvements to calculation time can also be achieved by employing adaptive integration methods: either by adaptively filtering the number of auxiliary matrixes or by adaptively adjusting the integration step size.

Received: May 15, 2012



<sup>&</sup>lt;sup>†</sup>Center for Biophysics and Computational Biology, University of Illinois at Urbana–Champaign, Urbana, Illinois 61801, United States

<sup>&</sup>lt;sup>‡</sup>Department of Physics and Beckman Institute, University of Illinois at Urbana-Champaign, Urbana, Illinois 61801, United States

Besides an application to large photosynthetic systems, such as those found in cyanobacteria, plants, and artificial light harvesting,  $^{73-77}$  the HEOM method is applicable to a wide range of other quantum systems. Indeed, any process that can be described by a set of N discrete quantum states in contact with a bosonic environment can be modeled.

In the following section, we present the partitioning scheme and integration methods used to implement the HEOM, as well as performance benchmarks of our parallel hierarchy integrator *PHI*. [The program *PHI* is presently available via the Internet at http://www.ks.uiuc.edu/Research/phi.]

# 2. METHODS

Many systems can be modeled with an effective Hamiltonian  $^{78-80}$  that describes the subset of relevant states  $|n\rangle$ , with energies  $E_n$  and interactions  $V_{nm}$ , written as

$$H_0 = \sum_{n}^{N} E_n |n\rangle \langle n| + \sum_{n,m}^{N} V_{nm} |n\rangle \langle m|$$
(1)

At present, PHI accounts only for Hermitian effective Hamiltonian operators, and thereby assumes a single excitation subspace. Systems such as those in a biological context are embedded in a  $T=300~\rm K$  thermal environment. Such environment can be modeled as an infinite set of harmonic oscillators<sup>11</sup>

$$H_{\rm B} = \sum_{\xi} \left[ \frac{p_{\xi}^2}{2m_{\xi}} + \frac{m_{\xi}\omega_{\xi}^2 q_{\xi}^2}{2} \right] \tag{2}$$

The thermal bath is coupled to the states  $|n\rangle$  through the system—bath interaction term,

$$H_{SB} = \sum_{a}^{M} \hat{F}_{a} u_{a} \tag{3}$$

where  $u_a = \sum_{\xi} c_{a\xi} q_{\xi}$  with  $c_{a\xi}$  being the coupling strength of vibrational mode  $\xi$  to the system via operator  $\hat{F}_a$ . In the case that each state  $|n\rangle$  is independently coupled to the environment, M = N and  $\hat{F}_a = |a\rangle \langle a|$  holds, where  $|a\rangle$  denotes one of the states  $|n\rangle$  arising in eq 1. The system—bath coupling introduces a shift in the minimum energy positions of the bath coordinates  $q_{\xi}$ , which can be countered by the renormalization term

$$H_{REN} = \sum_{ab}^{M} \hat{F}_a \hat{F}_b \sum_{\xi} \frac{c_{a\xi} c_{b\xi}}{2m_{\xi} \omega_{\xi}^2} \tag{4}$$

In the case of system—bath coupling that is independent for each state  $|n\rangle$ , the renormalization term reduces to  $H_{REN} = \sum_a^N |a\rangle \langle a|\lambda_{av}$  where  $\lambda_a$  is the bath reorganization energy ( $\lambda_a = \sum_{\xi} c_{a\xi}^2 / (2m_{\xi}\omega_{\xi}^2)$ ). The total Hamiltonian is thus given by  $H_T = H_S + H_B + H_{SB}$ , where  $H_S = H_0 + H_{REN}$  is the renormalized system Hamiltonian

The bath degrees of freedom are not of interest and, thus, are traced out of the dynamics to calculate the bath-averaged density matrix evolution as

$$\hat{\rho}(t) = \frac{\operatorname{tr}_{B} \left\{ \int e^{-i\mathcal{L}_{T}t/\hbar} \hat{\rho}(0) \otimes e^{-\beta H_{B}} dt \right\}}{\operatorname{tr}_{B} \left\{ e^{-\beta H_{B}} \right\}} = \langle \mathcal{U}(t) \rangle_{B} \hat{\rho}(0)$$
(5)

where  $\beta = 1/(k_BT)$ . Equation 5 corresponds to the so-called factorized initial condition that does not include initial

correlations between system and environment. Although initial correlations between system and environment would not be present in the case of instantaneous photoexcitation, <sup>61</sup> they can be included when modeling other processes using the HEOM. <sup>59,65</sup> Once the thermal average is performed, the influence of the environment enters only through the bath correlation functions, which are given by <sup>4</sup>

$$C_{ab}(t) = \langle u_a(t)u_b(0)\rangle_B = \frac{1}{\pi} \int_{-\infty}^{\infty} d\omega J_{ab}(\omega) \frac{e^{-i\omega t}}{1 - e^{-\beta\hbar\omega}}$$
(6)

where the spectral density  $J_{ab}(\omega)$  is given by

$$J_{ab}(\omega) = \frac{\pi}{2} \sum_{\xi} \frac{c_{a\xi} c_{b\xi}}{m_{\xi} \omega_{\xi}} \delta(\omega - \omega_{\xi})$$
 (7)

Because the coupling of environmental fluctuations to off-diagonal components in the system Hamiltonian are typically smaller than the coupling to diagonal components, i.e.  $|C_{ab}| \ll |C_{aa}|$ , they are usually ignored. <sup>54</sup> In the present work, only diagonal coupling to the environment is taken into account. Currently, only a few methods <sup>55–58,60,61</sup> offer numerically

Currently, only a few methods<sup>55–58,60,61</sup> offer numerically tractable equations of motion for the solution of eq 5 for system sizes as they arise in the case of pigment systems of photosynthetic light harvesting. The hierarchy equations of motion<sup>58–63,66,67,69,71,81</sup> (HEOM) is computationally expensive, but nevertheless furnishes an attractive method, because of its applicability across a broad range of interaction scenarios.<sup>34–36,66,69,72,80–86</sup>

**Correlation Functions.** The HEOM arise by exploiting bath correlation functions  $C_{ab}(t)$  described by sums of exponentially decaying terms. The HEOM work particularly well when the spectral density arising in eqs 6 and 7 can be expressed as a so-called Drude spectral density, which is given by

$$J_a(\omega) = 2\lambda_a \left( \frac{\omega \gamma_a}{\omega^2 + \gamma_a^2} \right) \tag{8}$$

where  $\lambda_a = \int \mathrm{d}\omega (J_a(\omega)/(\pi\omega))$  is the bath reorganization energy that determines the system—bath interaction strength, and  $1/\gamma_a$  is the bath response time. The Drude spectral density describes overdamped harmonic oscillator modes  $\xi$ . The correlation function associated with the Drude spectral density is <sup>69</sup>

$$C_a(t) = \sum_{k=0}^{\infty} c_{ak} \exp(-\nu_{ak}t)$$
(9)

where  $\nu_{a0} = \gamma_{av} \ \nu_{ak \ge 1} = 2\pi k/\beta \hbar$  are the Matsubara frequencies <sup>64</sup> and the coefficients  $c_{ak}$  are

$$c_{a0} = \gamma_a \lambda_a \left[ \cot \left( \frac{\beta \hbar \gamma_a}{2} \right) - i \right]$$
 (10)

$$c_{ak\geq 1} = \frac{4\lambda_a \gamma_a}{\beta \hbar} \left( \frac{\nu_{ak}}{\nu_{ak}^2 - \gamma_a^2} \right) \tag{11}$$

The summation to infinity in eq 9 must be truncated at a finite level, which is achieved by exploiting that beyond some finite K,  $\nu_{aK} \exp(-\nu_{aK}t) \approx \delta(t)$ .

The expansion of the correlation function using Matsubara frequencies (eqs 9 and 11) is not the only possible expansion, and recent work has shown that alternative expansions can yield better results for low cut-offs K.

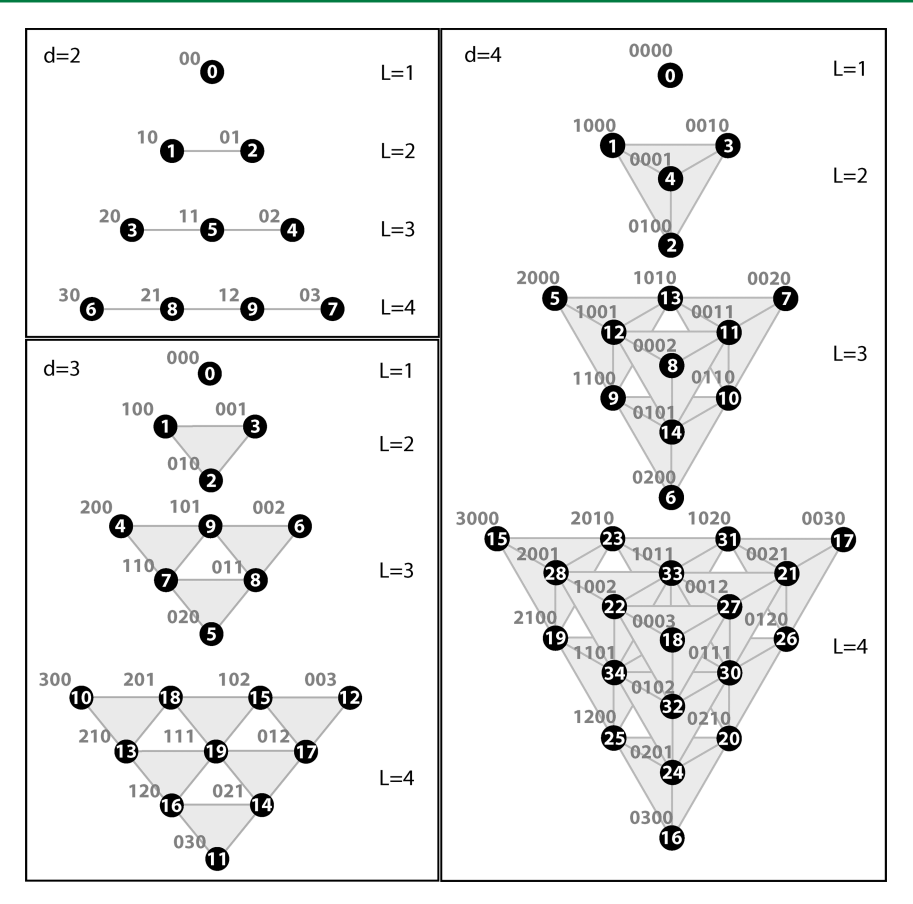


**Figure 1.** The first four hierarchy levels of Pascal's *d*-simplices for d = M(K + 1) = 2, 3, and 4. Each circle corresponds to a single ADM, with the corresponding index vectors **n** shown in blue text. The numbering inside the circles corresponds to the scheme described later in the hierarchy generation algorithm in Chart 1. The shaded regions indicate which ADMs are at the same level. The connectivity of the ADMs to those in the levels above and below is not shown.

In principle, one can also employ correlation functions for underdamped harmonic oscillators, namely, ones of the form  $C(t) = c \exp(-\gamma t) \cos(\Omega t)$ , to derive the HEOM,  $^{89-91}$  thus enabling the use of arbitrary, multipeaked spectral densities through, e.g., a Meier—Tannor decomposition.  $^{92}$  The Lorentzian peaks in such spectral densities, however, lead to many more terms in the HEOM which are only valid to second-order equations in system—bath coupling, such that, in practice, only Drude spectral densities are employed.  $^{90,91}$  At present, *PHI* treats spectral densities consisting of single or sums of Drude spectral densities.

**Hierarchy Equations of Motion.** In deriving the HEOM, each exponential term in eq 9 leads to the introduction of a set of operators,  $\hat{\rho}_{\mathbf{n}}$ , called auxiliary density matrices (ADMs). The  $\hat{\rho}_{\mathbf{n}}$  are indexed by a vector  $\mathbf{n}=(n_{10},...,n_{1K},...,n_{M0},...,n_{MK})$ . The equations of motion, which couple the ADMs in a hierarchical structure, are  $^{34,35,61,71}$ 

$$\hat{\rho}_{\mathbf{n}} = -\frac{i}{\hbar} [\hat{H}_{S}, \hat{\rho}_{\mathbf{n}}] - \sum_{a=1}^{M} \sum_{k=0}^{K} n_{ak} \nu_{ak} \hat{\rho}_{\mathbf{n}} 
- \sum_{a=1}^{M} \left( \frac{2\lambda_{a}}{\beta \hbar^{2} \gamma_{a}} - \sum_{k=0}^{K} \frac{c_{ak}}{\hbar \nu_{ak}} \right) [\hat{F}_{a}, [\hat{F}_{a}, \hat{\rho}_{\mathbf{n}}]] 
- i \sum_{a=1}^{M} [\hat{F}_{a}, \sum_{k=0}^{K} \hat{\rho}_{\mathbf{n}_{ak}^{+}}] 
- \frac{i}{\hbar} \sum_{a=1}^{M} \sum_{k=0}^{K} n_{ak} (c_{ak} \hat{F}_{a} \hat{\rho}_{\mathbf{n}_{ak}^{-}} - \hat{\rho}_{\mathbf{n}_{ak}^{-}} \hat{F}_{a} c_{ak}^{*})$$
(12)

Each ADM with index  $\mathbf{n}$  is coupled to ADMs with indices  $\mathbf{n}_{ak}^{\perp} = (n_{10},...,n_{ak}\pm 1,...,n_{MK})$ . Since there are no negative indices  $n_{ak}$  arising in the derivation of the HEOM,  $^{67}$  any ADM with a negative value for any  $n_{ak}$  is set to zero. The system density matrix  $\hat{\rho}$  is the density matrix with index vector  $\mathbf{n} = 0$ . Each density matrix in the hierarchy is assigned to a hierarchy level  $L = \sum_{a=1}^{M} \sum_{k=0}^{K} n_{ak}$ . The coupling of the HEOM leads to a structure that can be visualized as a Pascal's d-simplex, where d = M(K+1). Example hierarchies for d = 2, 3, and 4 are shown Figure 1.

The number of matrices rapidly increases with hierarchy level L (Figure 2) and, in principle, is infinite. The ADMs account for the non-Markovian extent of the dynamics, meaning that more ADMs are needed to capture dynamics with greater non-Markovian character. Because of this behavior, however, a natural truncation  $L_{\rm T}$  can be chosen such that  $L_{\rm T}$   $\min_{ak} (\nu_{ak}) \gg \omega_{\rm max}$  where  $\omega_{\rm max}$  is the maximum oscillation frequency in the system,

# Chart 1. Pseudo-Code Necessary to Generate Index Vectors n for Any Pascal's d-Simplex, Where d = M(K + 1) for the HEOM, up to a Specified Truncation Level<sup>a</sup>

"Operator legend: (=), scalar assignment operations; (:=) vector assignment operations.

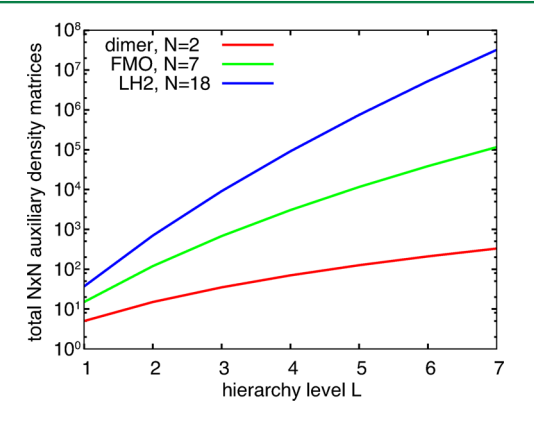


**Figure 2.** Total number of ADMs with increasing hierarchy level L for a pigment dimer, for the Fenna–Mathews–Olson (FMO) complex<sup>80</sup> and for light-harvesting complex 2 (LH2).<sup>34</sup>

without compromising the dynamics. Employing such truncation is often unfeasible due to computational limitations and, thus, convergence needs to be checked for each system to arrive at feasible values of  $L_{\rm T}$ .

Having chosen a truncation level  $L_{\rm T}$ , the manner in which the HEOM are cutoff must also be specified. There are two ways to truncate the HEOM, either with so-called "time nonlocal (TNL) truncation", which sets all ADMs in levels  $L_{\rm T}$  or greater to zero, for with the so-called "time-local (TL) truncation", which employs the Markovian approximation for ADMs in level  $L_{\rm T}$ . In case of the Markovian approximation, it is assumed that, for all ADMs with  $L=L_{\rm T}-1$ ,

$$\sum_{k=0}^{K} \hat{\rho}_{\mathbf{n}_{ak}^{+}} \approx -i(\hat{Q}_{a}^{K}(t)\rho_{\mathbf{n}} - \rho_{\mathbf{n}}\hat{Q}_{a}^{K}(t)^{\dagger})$$
(13)

where

$$\hat{Q}_{a}^{K}(t) = \int_{0}^{t} \left( \sum_{k=0}^{K} c_{ak} \exp(-\nu_{ak}\tau) \right) \exp\left(-\frac{i}{\hbar} H_{S}\tau\right) \times \hat{F}_{a} \exp\left(\frac{i}{\hbar} H_{S}\tau\right) d\tau$$
(14)

It has been shown that TNL truncation produces spurious peaks in absorption spectra<sup>66,71</sup> and, thus, TL truncation should be employed whenever possible.

### 3. NUMERICAL INTEGRATION OF HEOM

The HEOM present a significant computational challenge for all systems but one: a two-state system. Within single pigment—protein complexes in photosynthetic systems, pigment numbers lie typically between 6 and 90, depending on species and growth conditions. To overcome the issues of poor scaling with system size and truncation (Figure 2), and because of the highly coupled nature of the equations, the HEOM must be implemented computationally in the most efficient manner. This section describes the implementation of the HEOM in the parallel hierarchy integration software *PHI* capable of calculating excitation dynamics for systems containing up to 50 pigments at permissible truncation levels.

**Adaptive Integration.** Since the HEOM describe thermally averaged time evolution, the ADMs will exponentially approach, in the absence of an external driving field, a steady state. Any initial state of the system will relax to a steady state, leading during the relaxation to increasingly smaller changes in time of the elements of each ADM.

Shi et al. <sup>69</sup> proposed a rescaling of the ADMs that permits an automatic removal of the ADMs while integrating the HEOM. During integration, the ADMs are adaptively removed when their maximum absolute value is less than a defined filter accuracy  $\delta_F$ . This filtering greatly reduces the memory requirements for integrating the HEOM for moderate-sized systems, <sup>69,72</sup> but can lead to artifacts for choices of  $\delta_F$  values that are too large.

By employing the same rescaling of the ADMs as that employed by Shi et al., <sup>69</sup> one can exploit the damped dynamics by integrating the HEOM with an adaptive time step. Among the many adaptive integration methods, the Runga–Kutta–Fehlberg 4/5 (RKF45) method<sup>94</sup> stands out as most practical, because it is a fifth-order integration algorithm that does not require recalculation of a time step with a different step size in order to evaluate the integration error. The method, instead, reuses the interim Runga–Kutta steps to also compute a fourth-order integration step; at the end of a single time step, the fourth-order time step calculation is compared with the fifth-order time step calculation and the step is kept or discarded according to a tolerance  $\delta_I$  and the step size is increased or reduced accordingly.

Adaptive integration by the RKF45 algorithm requires six evaluations of the equations of motion, compared to four evaluations when using Runga—Kutta 4 (RK4) fixed time-step integration. The additional computation per RK45 step, compared to a RK4 step, however, typically results in an order-of-magnitude decrease in the number of integration steps, compared to RK4, with an overall reduction in total computation time. Rapid initial dynamics, as well as long-time relaxation to the steady state, are both covered efficiently, with an overall short calculation time and a predefined integration error tolerance.

Adaptive time-step integration, however, cannot typically be used in conjunction with the adaptive ADM filtering method of Shi et al., because the latter introduces artifacts in the time evolution of the ADMs that result in the adaptive integration method taking smaller time steps than without the automatic filtering. As will be shown in the Results section below, suitable choices of  $\delta_F$  and  $\delta_I$  values still result in speed-up, within an acceptable error.

**Partitioning.** Central to efficient integration of the HEOM is the use of parallel computing. Unfortunately, large numbers of processors linked in computer clusters (i.e., in distributed memory computers) with a low network bandwidth cannot be used, since the HEOM, particularly for systems of many

pigments, are extremely coupled, and require a high bandwidth for interprocessor communication. However, this communication cost can be managed by employing multiple threads running on a multiprocessor, shared-memory computer.

In principle, it is relatively straightforward to assign *P* processing threads (where each thread is an independently executing process able to communicate with other threads and access the same shared memory) to a set of ADMs. Integration then proceeds by computing and applying the integration updates from the HEOM in parallel, pausing between each step to synchronize data between the *P* threads. The communication overhead due to the highly coupled nature of the HEOM means that even with modern symmetric multiprocessing (SMP) hardware, however, the ADMs must be well-partitioned to avoid memory contention and maximize use of memory bandwidth available to each processor.

An algorithm for generating the index vectors  $\mathbf{n}$  of the ADMs and, thus, the vertices of the associated Pascal's d-simplex, is given in Chart 1. The partitioning algorithm (Chart 2) employs

# Chart 2. Algorithm to Partition the Vertices of a Pascal's *d*-Simplex into *P* Sets, Minimizing Interset Connections While Ensuring that the Numbers of Vertices in Each Set Differ by, at Most. 1<sup>a</sup>

```
1 d=M*(K+1)
2 numVertsInSet[] := vector of P zeros;
3 verticesInSet[0][0] = 0;
4 numVertsInSet[0] = 1;
5 for vertexID = 1 to d
6 setID = (vertexID - 1) modulo P;
7 verticesInSet[setID][numVertsInSet[setID]] = vertexID;
8 numVertsInSet[setID] += 1;
9 nextCornerVertexID += vertexID + d;
1 for k = 2 to truncationLevel-1
11 verticesInSet[setID][numVertsInSet[setID]] = nextCornerVertexID;
12 numVertsInSet[setID] += 1;
13 nextCornerVertexID += numVertsInSet[setID]] = nextCornerVertexID;
14 for vertexID = 2 d+1 to totalNumVertices-1
15 if vertexID not in verticesInSet[[1]]
16 if P > d and vertexID < P +d+1
17 setID = vertexID modulo P;
18 verticesInSet[setID][numVertsInSet[setID]] = vertexID;
19 numVertsInSet[setID] += 1;
20 else
21 connectionsToSet[] := vector of P zeros;
22 for j = 0 to d-1
23 tupIndexVector[] := indexVectorList[vertexID][];
24 tupIndexVector[] := indexVectorList[vertexID][];
25 tupVertexID = vertex associated with tmpIndexVector
26 setID = id of set containing tmpVertexID
27 connectionsToSet[setID] += 1;
28 connMax[] := all p where connectionsToSet[p] == max(connectionsToSet[]);
29 setID = p in connMax[] where numVertsInSet[p] == min(numVertsInSet[]);
30 if numVertsInSet[setID] >= all(totalNumVertices / P)
31 setID = id where numVertsInSet[setID] = vertexID;
32 verticesInSet[setID] >= all(totalNumVertics) = lindexID = vertexID;
33 numVertsInSet[setID] >= all(totalNumVertics) = lindexID = vertexID;
34 numVertsInSet[setID] >= all(totalNumVertics) = lindexID = vertexID;
35 numVertsInSet[setID] >= all(totalNumVertics) = lindexID = vertexID;
36 numVertsInSet[setID] >= all(totalNumVertics) = lindexID = vertexID;
36 numVertsInSet[setID] >= all(totalNumVertsInSet[]);
37 numVertsInSet[setID] >= all(totalNumVertsInSet[]);
38 numVertsInSet[setID] >= all(totalNumVertsInSet[]);
39 numVertsInSet[setID] >= all(totalNumVertsInSet[]);
30 numVertsInSet[setID] >= lindexID = min(numVertsInSet[]);
31 numVertsInSet[setID] >= lindexID = min(numVertsInSet[]);
32 verticesInSet[setID] >= lindexID = vertexID;
31 numVert
```

"The algorithm employs the results of the index vector generation code in Chart 1. Operator legend: (=), scalar assignment operations; (:=), vector assignment operations; and (= =), test for equality.

the numbering scheme used in Chart 1 to assign each vertex to a set such that the number of interset edges is minimal while ensuring that each set contains almost the same number of vertices. An example of the partitioning of a hierarchy of ADMs associated with a Pascal's 3-simplex is shown in Figure 3. The partitioning algorithm presented here reduces the interset connections, compared to either block- or cyclic-partitioning schemes often employed in parallel programming. Assigning each set to a separate thread and, crucially, instructing each thread to allocate the memory required to store the ADMs in its set, reduces interprocessor memory contention and dramatically improves the performance of the parallel HEOM integration software *PHI*.

# 4. RESULTS

Excitation dynamics is a key process in photosynthetic light harvesting. Excitation must be transferred over many nanometers

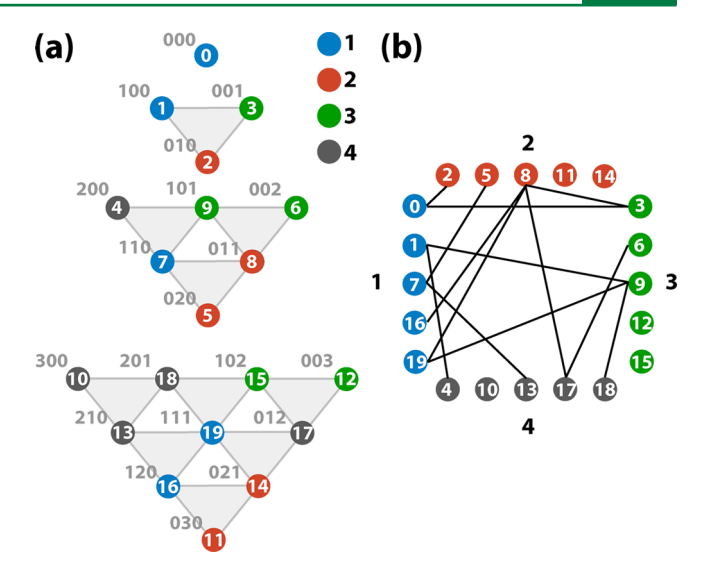


**Figure 3.** Partitioning of a Pascal's 3-simplex into four sets. The partitioning (a) results in each subset containing five vertices, with (b) 13 edges crossing between subsets.

for light energy to be utilized by the cell. Since the excitation lifetime is rather short—namely, only 1 ns—transfer must be fast to be efficient. In purple photosynthetic bacteria, such as *Rps. molischianum*, the needed efficiency is achieved by placing pigment molecules into ringlike structures, as shown in Figure 4,

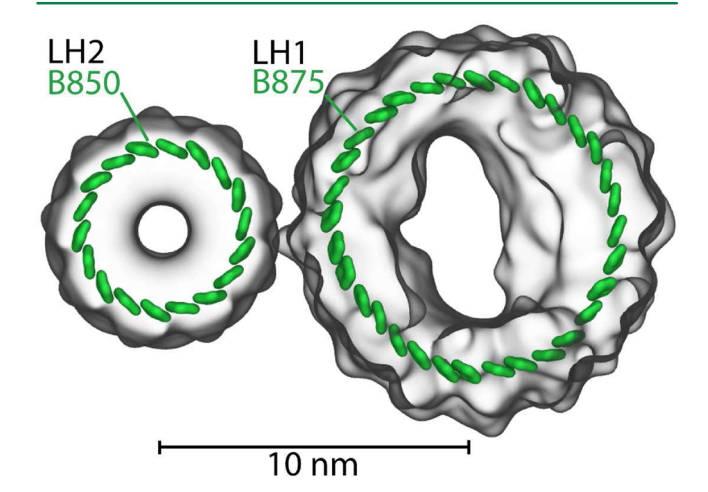


**Figure 4.** Molecular graphics depictions of the pigment–protein complexes: light-harvesting complex 2 (**LH2**) and light-harvesting complex 1 (**LH1**). Shown are the 18 pigments that form the B850 ring of **LH2** and the 32 pigments that form the B875 ring of **LH1**. 32,95

and transferring excitation between the ringlike structures. Light energy typically absorbed by light harvesting complex 2 (LH2, B850 ring)<sup>32</sup> is passed by intercomplex excitation transfer to light-harvesting complex 1 (LH1, B875 ring)<sup>95</sup> prior to charge separation at the photosynthetic reaction center.<sup>17</sup> The closepacking arrangements and pigment orientations in the ringlike structures result in quantum coherence that enhances excitation transfer between the rings.<sup>39</sup>

Here, we present the effects of employing different HEOM integration parameters and methods. First, we examine the effect of adaptive time-step integration for a pigment dimer and for an 18-pigment ring, the so-called B850 ring in LH2.<sup>32</sup> Second, we employ the B850 ring as a model system to investigate the

parallel performance of *PHI*. Finally, the transfer of excitation between the two ring structures—the B850 ring and the 32-pigment B875 ring in LH1<sup>95</sup> (shown in Figure 4)—is computed.

**Effect of Integration Time Step and Method.** Below, results are presented to demonstrate the effect of fixed and adaptive time steps on integration speed and accuracy. First, a model dimer system is employed to highlight the importance of choosing an appropriate time step. The dimer is specified by  $H_S = \Delta E \hat{\sigma}_z + V \hat{\sigma}_x$ , where  $\Delta E = 100 \text{ cm}^{-1}$  and  $V = 200 \text{ cm}^{-1}$ , the reorganization energies are given as  $\lambda_1 = \lambda_2 = 50 \text{ cm}^{-1}$ , and the response frequencies are  $\gamma_1 = \gamma_2 = 1/(0.1 \text{ ps})$ ;  $\hat{\sigma}_z$  and  $\hat{\sigma}_x$  are Pauli matrices. As can be seen from Figure 5, using a time step that is

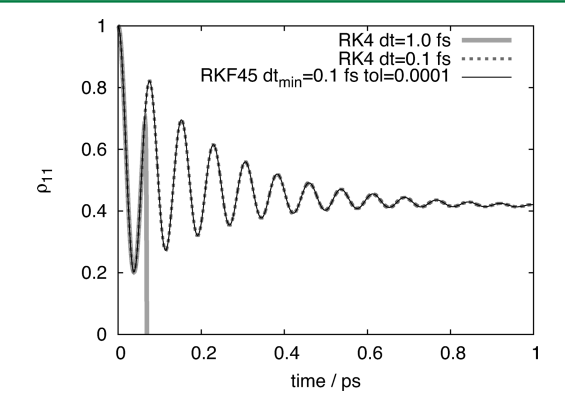


**Figure 5.** Comparison of HEOM integration schemes. Integration on four processors (CPU cores) took 0.23 min for Runga–Kutta 4 (RK4) integration, using 0.1 fs timesteps, and 0.03 min using Runga–Kutta–Fehlberg 4/5 (RKF45) adaptive integration with a minimum time step of 0.1 fs and a tolerance of 0.0001.

too large can rapidly cause integration errors. Fortunately, in such a simple system, such gross errors are easy to detect and rectify. For larger systems, however, finding the optimum time step can be time-consuming. By employing the RKF45 adaptive time-step integration method (see the Methods section), such effort can be avoided and achieving greatly improved performance becomes much easier.

Effect of Integration Time Step and Method. To examine the accuracy and speed of different integration options, we consider the case of light excitation of one of the primary absorbing states of the B850 ring of pigments in light-harvesting complex 2 (LH2). The excitation dynamics of the 18-pigment B850 ring was previously characterized,<sup>34</sup> and calculations are repeated here to investigate the effect of different integration methods. The resulting exciton dynamics is shown in Figure 6 for the reference calculation; Table 1 presents the accuracy and computation time of adaptive and nonadaptive integration methods. One can clearly discern that the Shi et al. adaptive filtering dramatically reduces computation time in the case of Runga-Kutta 4 (RK4) integration. Excellent performance can also be achieved using RKF45 adaptive time-step integration, with typically shorter calculation times and improved accuracy than needed for the other methods listed. Both adaptive methods can be combined for optimal performance as long as the RKF45 tolerance is larger than the ADM filter accuracy, i.e., for  $\delta_I > \delta_E$ ; otherwise, longer computation times result. In general, optimal RK4 time step and ADM filter accuracy are both dependent on system parameters and, thus, require time-consuming benchmark calculations. Employing RKF45 adaptive time-step integration yields significant performance gains without prior benchmarks.

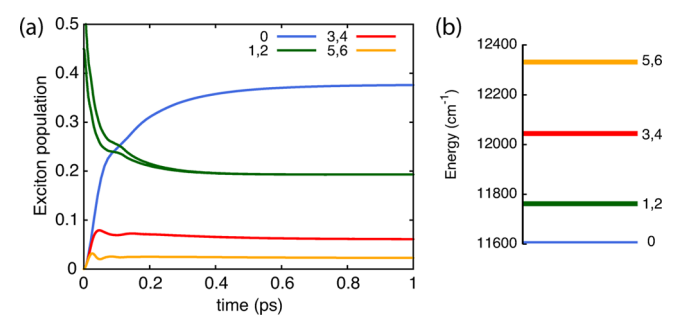


**Figure 6.** Exciton dynamics of the seven lowest-energy exciton states of the B850 ring in **LH2** with the initial state given by a superposition of the degenerate 850-nm exciton states 1 and 2 ((a) populations of associated states and (b) energies of associated states).

**Parallel Performance.** The key to employing the HEOM to calculate excitation dynamics in large pigment systems is scalability to many processors. With efficient scaling, the size of the problem that can be treated depends only on the size of the computer available and is not limited by the speed of a single processor. To endow *PHI* with optimal scaling capabilities, three steps were taken: (1) memory assignment was changed from being initially assigned to a single large block to being assigned to separate smaller blocks, one for each integration thread; (2) the partitioning of the ADMs was done satisfying minimum interthread communication; (3) each thread was assigned to a specific processor. The effect of the three steps, shown in Figure 7, is a greater than 3-fold reduction in calculation time when employing 48 cores, and significantly better scaling, compared to cyclic decomposition.

A significant boost in parallel performance is thus gained from the hierarchical partitioning scheme detailed in Charts 1 and 2. The increased computational work arising from increasing the K truncation can be countered with the parallel efficiency of PHI. The performance saturation seen around 48 cores in Figure 7 indicates that interprocessor communication is still a bottleneck and any scheme to reduce this bottleneck will result in further performance improvement. The rapid bandwidth saturation that arises even with the high-bandwidth processor-memory bus (42 GB/s for the AMD Magny-Cours CPU) suggests that parallel performance on a distributed memory computer is relatively poor.

**Excitation Transfer between LH2 and LH1.** With the improvements in scalability and calculation time for integration of the HEOM described above, one can model excitation transfer between two large pigment—protein complexes: **LH2** and **LH1** (see Figure 4).

In the photosynthetic light-harvesting apparatus of purple bacteria, most excitation transfer steps occur between the 18-pigment B850 ring in **LH2** and the 32-pigment B875 ring in **LH1**.  $^{18,19,32}$  In order to describe this transfer, one must account for N=50 pigments. Modeling a system of this size is not possible with a single-processor implementation of the HEOM; instead, it requires *PHI* running on a parallel computer.

The parameters describing the B850 and B875 Hamiltonians are taken from ref 48, with bath parameters  $\lambda_n = \lambda = 180~{\rm cm}^{-1}$  and  $1/\gamma_n = 1/\gamma = 100$  fs, a choice that had been shown to reproduce experimental spectra. The population of an initially excited **LH2** complex is shown in Figure 8 for different truncations and intercomplex separation distances. The results show that TL truncation with a cutoff of  $L_T = 3$  yields a population decay close to that of an  $L_T = 5$  cutoff. The lower truncation requires 50 MB

Table 1. Accuracy and Performance of Different Integration Methods for Calculating the Excitation Dynamics of the B850 Pigments of LH2 with Parameters and Truncation (as Given in Ref 34)

integration method	ADM filter, $^a$ $\delta_{\scriptscriptstyle F}$	integration tolerance, ${}^b\delta_I$	integration step size (fs)	average error <sup>c</sup>	calculation time (min)
RK4			0.1	0	920
RK4			1.0	$2.0 \times 10^{-7}$	91.8
RK4			2.0	$5.4 \times 10^{-7}$	46.0
RK4	$10^{-6}$		1.0	$2.0 \times 10^{-7}$	83.9
RK4	$10^{-6}$		2.0	$5.5 \times 10^{-7}$	42.1
RK4	$10^{-4}$		1.0	$7.8 \times 10^{-6}$	43.4
RK4	$10^{-4}$		2.0	$1.1 \times 10^{-5}$	25.7
RK4	$10^{-2}$		1.0	$2.7 \times 10^{-3}$	34.5
RK4	$10^{-2}$		2.0	$2.9 \times 10^{-3}$	21.9
RKF45		$10^{-6}$	$1.0 \rightarrow 7.5$	$6.1 \times 10^{-7}$	35.6
RKF45		$10^{-4}$	$1.0 \rightarrow 7.4$	$8.2 \times 10^{-7}$	33.3
RKF45		$10^{-2}$	$1.0 \rightarrow 8.1$	$1.2 \times 10^{-6}$	33.1
RKF45	$10^{-6}$	$10^{-6}$	$1.0 \rightarrow 2.0$	$3.3 \times 10^{-7}$	66.1
RKF45	$10^{-6}$	$10^{-4}$	$1.0 \rightarrow 4.6$	$6.7 \times 10^{-7}$	34.1
RKF45	$10^{-6}$	$10^{-2}$	$1.0 \rightarrow 8.1$	$9.9 \times 10^{-7}$	33.0
RKF45	$10^{-4}$	$10^{-6}$	$0.6 \rightarrow 1.2$	$7.8 \times 10^{-6}$	71.0
RKF45	$10^{-4}$	$10^{-4}$	$1.0 \rightarrow 2.4$	$1.1 \times 10^{-5}$	34.4
RKF45	$10^{-4}$	$10^{-2}$	$1.0 \rightarrow 4.6$	$1.5 \times 10^{-5}$	24.1
RKF45	$10^{-2}$	$10^{-6}$	$0.3 \rightarrow 1.2$	$2.0 \times 10^{-3}$	93.2
RKF45	$10^{-2}$	$10^{-4}$	$0.7 \rightarrow 2.4$	$2.8 \times 10^{-3}$	50.9
RKF45	$10^{-2}$	$10^{-2}$	$1.0 \rightarrow 3.8$	$3.3 \times 10^{-3}$	27.9

<sup>&</sup>lt;sup>a</sup>Filter constant for Shi et al. adaptive ADM filtering. <sup>69</sup> Integration tolerance for Runga–Kutta–Fehlberg 4/5 (RKF45) adaptive integration. <sup>94</sup> Average absolute error in each element of the system density matrix per time step, defined as follows: error =  $(N^2N_t)^{-1}\sum_{n}^{N_t}\sum_{i,j}^{N_t}|\rho_{ij}(t_n) - \rho_{ij}^{\text{ref}}(t_n)|$ .

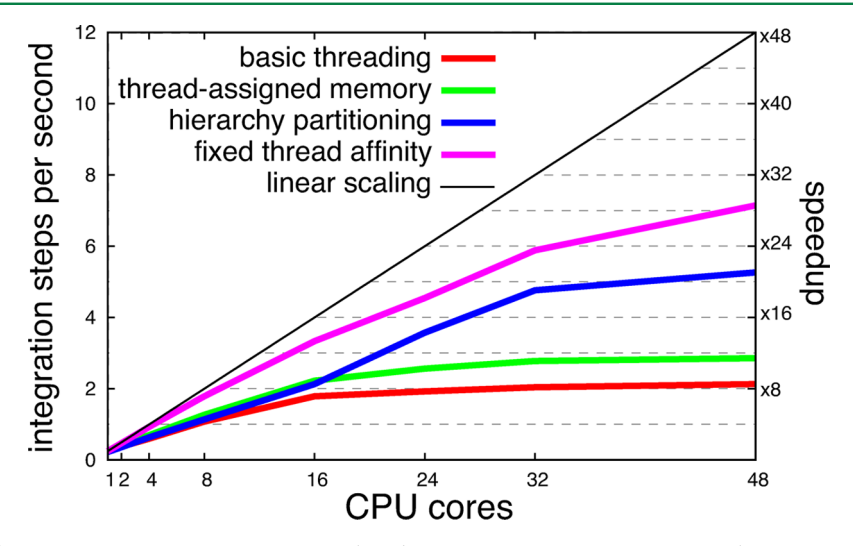


Figure 7. Parallel scaling of PHI on a 48-core AMD Magny-Cours shared-memory computer running Linux. The system employed for benchmarking is the set of 18 pigments in the B850 ring of LH2 with  $L_T = 4$  and K = 1. "Basic partitioning" refers to a cyclic partitioning of ADMs and the memory for all ADMs being assigned to a consecutive block; "thread-assigned memory" refers to instructing each thread to perform memory assignment for its set of ADMs in the cycling partitioning scheme; "hierarchy partitioning" refers to employing the partitioning described in Charts 1 and 2 and using thread-assigned memory; "fixed thread affinity" refers to employing the partitioning scheme in Charts 1 and 2, using thread-assigned memory and instructing the operating system's thread scheduler to affix each thread to a particular processor such that no thread migration occurs.

of memory to store the hierarchy of ADMs and 415 MB of memory for RKF45 integration; however, the higher truncation requires 12 GB of memory to store the hierarchy of ADMs and 96 GB of memory for RKF45 integration.

The excitation transfer time can be calculated by fitting a simple kinetic model that describes the excitation transfer between B850 and B875 BChl rings (see Figure 8), namely,

$$\frac{\mathrm{d}P_{\mathrm{B850}}}{\mathrm{d}t} = -\frac{P_{\mathrm{B850}}}{\tau_{\mathrm{B850} \to \mathrm{B875}}} + \frac{1 - P_{\mathrm{B850}}}{\tau_{\mathrm{B875} \to \mathrm{B850}}} \tag{15}$$

In our calculations, we assumed three separations between the proteins **LH1** and **LH2** holding the B875 and B850 BChl rings, respectively, namely, edge—edge separations of 2 nm, 1 nm, and 0 nm (contact). In case of contact, transfer times (summarized in Table 2) are  $\tau_{\text{B850}\rightarrow\text{B875}}=4.1$  ps and  $\tau_{\text{B875}\rightarrow\text{B850}}=18.4$  ps; interprotein separations of 1 and 2 nm result in 260% and 590% longer transfer times, respectively.

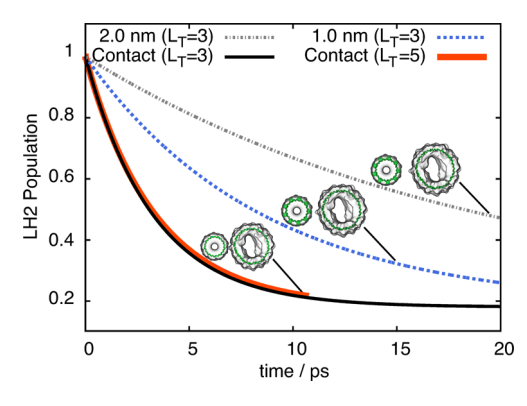


Figure 8. Total excited-state population of LH2 reflecting intercomplex excitation transfer from LH2 to LH1 at different protein (LH2)—protein (LH1) edge—edge separations.

Table 2. Excitation Transfer Times between the B850 Pigments in LH2 and the B875 Pigments in LH1

hierarchy truncation	interprotein distance (nm)	$ au_{ ext{B850}  o  ext{B875}}  ag{ps}$	$ au_{ ext{B875}  ightarrow  ext{B850}}  ag{ps}$
$L_{\mathrm{T}} = 5$	0.0	4.1	18.4
$L_{\mathrm{T}} = 3$	0.0	4.0	18.1
$L_{\mathrm{T}} = 3$	1.0	10.4	46.7
$L_{\rm T} = 3$	2.0	23.6	105

#### 5. CONCLUSION

The hierarchy equations of motion (HEOM) employ a highly coupled set of density matrices to calculate the noise-averaged time evolution of a quantum system coupled to a thermal environment. The large number of matrices required to model multipigment systems using the HEOM has restricted the method to systems with only very few pigments. By employing adaptive numerical integration methods (hierarchy filtering of Shi et al.<sup>69</sup> and adaptive time-step integration<sup>94</sup>) and a novel hierarchy partitioning scheme, efficient scaling has been realized. The software implementation available in the PHI program can be run on parallel computers, allowing the HEOM to be solved for pigment numbers as large as those found in biological systems. The performance of PHI has been demonstrated here by investigating the accuracy of the adaptive integration methods and by applying PHI to model excitation transfer in a 50-pigment system, namely, the 18-BChl B850 ring in light-harvesting complex 2 (LH2) and the 32-BChl B875 ring in light-harvesting complex 1 (LH1) of purple photosynthetic bacteria. It was shown that excitation transfer between LH2 and LH1 practically occurs as a Poisson process (i.e., an incoherent hopping process, described by a single exponential decay of excited-state population). The excitation transfer times for LH2 -> LH1 and LH1 → LH2 were calculated for direct protein-protein contact, as well as for protein-protein separations of 1 and 2 nm. Resulting transfer rates compare well with observations<sup>23</sup> and generalized Förster theory results; 78 the latter agreement should be considered an a posteriori justification of generalized Förster theory.

The efficient parallel implementation of the HEOM makes it possible to model even larger light-harvesting systems than those studied here, such as photosystem 1 and photosystem 2 in cyanobacteria and plants, <sup>73,74</sup> as well as conjugated polymers <sup>76</sup> and pigment dendrimers <sup>77</sup> used in artificial light harvesting. The current implementation of the HEOM would also benefit the calculation of exact quantum dynamics in Wigner space, which

recently has been shown to also be computationally challenging, because of large memory requirements. In addition, the general applicability of the HEOM allows PHI to be used for investigations of other open quantum systems such as charge-transfer reactions,  $^{90}$  e.g., in DNA $^{97}$  and in the photosynthetic reaction center,  $^{98}$  or coherently coupled spin systems such as those employed in quantum computing.  $^{99-101}$ 

# AUTHOR INFORMATION

# **Corresponding Author**

\*E-mail: kschulte@ks.uiuc.edu.

#### Notes

The authors declare no competing financial interest.

# ACKNOWLEDGMENTS

The authors are grateful for insightful discussions with John Stone. Funding for J.S. and K.S. was provided by NSF Grant No. PHY0822613 and NIH Grant Nos. MCB-0744057 and P41-RR05969.

# REFERENCES

- (1) Hopfield, J. J. Proc. Natl. Acad. Sci. U.S.A. 1974, 71, 3640-3644.
- (2) Knox, R. S. In *Primary Processes of Photosynthesis*; Barber, J., Ed.; Elsevier: Amsterdam, 1977; pp 55–97.
- (3) Marcus, R. A.; Sutin, N. Biochim. Biophys. Acta 1985, 811, 265–322.
- (4) May, V.; Kühn, O. Charge and Energy Transfer Dynamics in Molecular Systems; Wiley-VCH: Berlin, 2000.
- (5) Förster, T. Ann. Phys. (Leipzig) 1948, 2, 55-75.
- (6) Redfield, A. IBM J. Res. Dev. 1957, 1, 19-31.
- (7) McLachlan, A. D. Mol. Phys. 1964, 8, 39.
- (8) Micha, D. A. J. Chem. Phys. 1983, 78, 7138-7145.
- (9) Haken, H.; Reineker, P. Z. Phys. A 1972, 249, 253-268.
- (10) Haken, H.; Strobl, G. Z. Phys. A 1973, 262, 135-148.
- (11) Caldeira, A. O.; Leggett, A. J. J. Ann. Phys. (N.Y.) 1983, 149, 374–456.
- (12) Yang, M.; Fleming, G. R. Chem. Phys. 2002, 282, 163-180.
- (13) Renger, T.; Marcus, R. J. Chem. Phys. 2002, 116, 9997.
- (14) Mukamel, S. Principles of Nonlinear Optical Spectroscopy; Oxford University Press: New York, 1995.
- (15) Weiss, U. Quantum Dissipative Systems; World Scientific Publishing Company: Singapore, 2008.
- (16) Breuer, H. P.; Petruccione, F. The Theory of Open Quantum Systems; Oxford University Press: New York, 2002.
- (17) Blankenship, R. E. Molecular Mechanisms of Photosynthesis; Blackwell Science: Malden, MA, 2002.
- (18) Sener, M. K.; Olsen, J. D.; Hunter, C. N.; Schulten, K. Proc. Natl. Acad. Sci., U.S.A. 2007, 104, 15723–15728.
- (19) Sener, M.; Strumpfer, J.; Timney, J. A.; Freiberg, A.; Hunter, C. N.; Schulten, K. *Biophys. J.* **2010**, *99*, 67–75.
- (20) Freiberg, A.; Godik, V. I.; Pullerits, T.; Timpmann, K. Biochim. Biophys. Acta 1989, 973, 93–104.
- (21) Visscher, K. J.; Bergstrom, H.; Sundström, V.; Hunter, C.; van Grondelle, R. *Photosyn. Res.* 1989, 22, 211–217.
- (22) Pullerits, T.; Visscher, K. J.; Hess, S.; Sundström, V.; Freiberg, A.; Timpmann, K. *Biophys. J.* **1994**, *66*, 236–248.
- (23) Hess, S.; Chachisvilis, M.; Timpmann, K.; Jones, M.; Fowler, G.; Hunter, C.; Sundström, V. *Proc. Natl. Acad. Sci. U.S.A.* **1995**, 92, 12333–12337.
- (24) Leegwater, J. A. J. Phys. Chem. 1996, 100, 14403-14409.
- (25) Sundström, V.; von Grondelle, R. In *Anoxygenic Photosynthetic Bacteria*; Blankenship, R. E., Madigan, M. T., Bauer, C. E., Eds.; Advances in Photosynthesis and Respiration; Springer: Dordrecht, The Netherlands, 2004; Vol. 2; pp 349–372.
- (26) van Grondelle, R.; Novoderezhkin, V. I. *Phys. Chem. Chem. Phys.* **2006**, *8*, 793–807.

- (27) Lee, H.; Cheng, Y.-C.; Fleming, G. R. Science 2007, 316, 1462–1465.
- (28) Pullerits, T.; Polivka, T.; Sundström, V. Ultrashort Laser Pulses Biol. Med. 2008, 11, 95–115.
- (29) Caruso, F.; Saikin, S. K.; Solano, E.; Huelga, S. F.; Aspuru-Guzik, A.; Plenio, M. B. *Phys. Rev. B* **2012**, *85*, 125424.
- (30) Linnanto, J.; Korppi-Tommola, J. Chem. Phys. 2009, 357, 171–180.
- (31) Caycedo-Soler, F.; Rodríguez, F. J.; Quiroga, L.; Johnson, N. F. New J. Phys. **2010**, *12*, 095008.
- (32) Hu, X.; Ritz, T.; Damjanović, A.; Schulten, K. J. Phys. Chem. B 1997, 101, 3854-3871.
- (33) Damjanović, A.; Kosztin, I.; Kleinekathoefer, U.; Schulten, K. Phys. Rev. E 2002, 65, 031919.
- (34) Strümpfer, J.; Schulten, K. J. Chem. Phys. 2009, 131, 225101.
- (35) Strümpfer, J.; Schulten, K. J. Chem. Phys. 2011, 134, 095102.
- (36) Hsin, J.; Strümpfer, J.; Sener, M.; Qian, P.; Hunter, C. N.; Schulten, K. New J. Phys. **2010**, *12*, 085005.
- (37) Huelga, S. F.; Rivas, A.; Plenio, M. B. *Phys. Rev. Lett.* **2012**, *108*, 160402.
- (38) Ishizaki, A.; Fleming, G. J. Phys. Chem. B 2011, 115, 6227-6233.
- (39) Strümpfer, J.; Sener, M.; Schulten, K. J. Phys. Chem. Lett. 2012, 3, 536–542.
- (40) Rebentrost, P.; Mohseni, M.; Aspuru-Guzik, A. J. Phys. Chem. B **2009**, 113, 9942–9947.
- (41) Plenio, M.; Huelga, S. New J. Phys. 2008, 10, 113019.
- (42) Caruso, F.; Chin, A.; Datta, A.; Huelga, S.; Plenio, M. J. Chem. Phys. 2009, 131, 105106.
- (43) Chin, A.; Datta, A.; Caruso, F.; Huelga, S.; Plenio, M. New J. Phys. **2010**, *12*, 065002.
- (44) Caruso, F.; Chin, A.; Datta, A.; Huelga, S.; Plenio, M. *Phys. Rev. A* **2010**, *81*, 062346.
- (45) Mohseni, M.; Rebentrost, P.; Lloyd, S.; Aspuru-Guzik, A. J. Chem. Phys. 2008, 129, 174106.
- (46) Rebentrost, P.; Mohseni, M.; Kassal, I.; Lloyd, S.; Aspuru-Guzik, A. New J. Phys. **2009**, *11*, 033003.
- (47) Rebentrost, P.; Chakraborty, R.; Aspuru-Guzik, A. J. Chem. Phys. **2009**, 131, 184102.
- (48) Hu, X.; Damjanović, A.; Ritz, T.; Schulten, K. *Proc. Natl. Acad. Sci. U.S.A.* **1998**, *95*, 5935–5941.
- (49) Timpmann, K.; Trinkunas, G.; Qian, P.; Hunter, C. N.; Freiberg, A. Chem. Phys. Lett. **2005**, 414, 359–363.
- (50) Trinkunas, G.; Freiberg, A. J. Luminesc. 2006, 119–120, 105–110.
- (51) Valkunas, L.; Janusonis, J.; Rutkauskas, D.; van Grondelle, R. J. Luminesc. 2007, 127, 269–275.
- (52) Janusonis, J.; Valkunas, L.; Rutkauskas, D.; van Grondelle, R. *Biophys. J.* **2008**, *94*, 1348–1358.
- (53) Olaya-Castro, A.; Lee, C. F.; Olsen, F. F.; Johnson, N. F. *Phys. Rev.* B **2008**, 78, 085115.
- (54) Freiberg, A.; Ratsep, M.; Timpmann, K.; Trinkunas, G. Chem. Phys. **2009**, 357, 102–112.
- (55) Prior, J.; Chin, A.; Huelga, S.; Plenio, M. Phys. Rev. Lett. 2010, 105, 50404.
- (56) Chin, A.; Rivas, Á.; Huelga, S.; Plenio, M. *J. Math. Phys.* **2010**, *51*, 092109.
- (57) Topaler, M.; Makri, N. Chem. Phys. Lett. 1993, 210, 448-457.
- (58) Tanimura, Y.; Kubo, R. J. Phys. Soc. Jpn. 1989, 58, 1199-1206.
- (59) Tanimura, Y. Phys. Rev. A 1990, 41, 6676-6687.
- (60) Ishizaki, A.; Tanimura, Y. J. Phys. Soc. Jpn. 2005, 74, 3131-3134.
- (61) Ishizaki, A.; Fleming, G. R. J. Chem. Phys. 2009, 130, 234111-10.
- (62) Yan, Y.; Yang, F.; Liu, Y.; Shao, J. Chem. Phys. Lett. 2004, 395, 216-221.
- (63) Xu, R. X.; Cui, P.; Li, X. Q.; Mo, Y.; Yan, Y. J. J. Chem. Phys. 2005, 122, 041103.
- (64) Yan, Y. J.; Xu, R. X. Annu. Rev. Phys. Chem. 2005, 56, 187.
- (65) Tanimura, Y. J. Phys. Soc. Jpn. 2006, 75, 082001.
- (66) Schröder, M.; Kleinekathöfer, U.; Schreiber, M. J. Chem. Phys. **2006**, 124, 084903.
- (67) Xu, R. X.; Yan, Y. J. Phys. Rev. E 2007, 75, 031107-11.

- (68) Ishizaki, A.; Tanimura, Y. J. Phys. Chem. A 2007, 111, 9269-9276.
- (69) Shi, Q.; Chen, L.; Nan, G.; Xu, R.; Yan, Y. J. Chem. Phys. 2009, 130, 084105-4.
- (70) Xu, R. X.; Tian, B. L.; Xu, J.; Yan, Y. J. J. Chem. Phys. 2009, 130, 074107-8.
- (71) Chen, L.; Zheng, R.; Shi, Q.; Yan, Y. J. Chem. Phys. 2009, 131, 094502.
- (72) Kreisbeck, C.; Kramer, T.; Rodriguez, M.; Hein, B. *J. Chem. Theor. Comput.* **2011**, 7, 2166–2174.
- (73) Wientjes, E.; Van Stokkum, I.; Van Amerongen, H.; Croce, R. *Biophys. J.* **2011**, *100*, 1372–1380.
- (74) Croce, R.; Van Amerongen, H. J. Photochem. Photobiol. B **2011**, 104, 142–153.
- (75) Scholes, G.; Fleming, G.; Olaya-Castro, A.; van Grondelle, R. *Nat. Chem.* **2011**. 3, 763–774.
- (76) Bolinger, J. C.; Traub, M. C.; Adachi, T.; Barbara, P. F. Science **2011**, 331, 565–567.
- (77) Imahori, H. J. Phys. Chem. B 2004, 108, 6130-6143.
- (78) Hu, X.; Ritz, T.; Damjanović, A.; Autenrieth, F.; Schulten, K. Q. Rev. Biophys. **2002**, 35, 1–62.
- (79) Şener, M.; Schulten, K. In *Energy Harvesting Materials*; Andrews, D. L., Ed.; World Scientific: Singapore, 2005; pp 1–26.
- (80) Ishizaki, A.; Fleming, G. R. Proc. Natl. Acad. Sci. U.S.A. 2009, 106, 17255.
- (81) Zhu, K.; Xu, R.; Zhang, H.; Hu, J.; Yan, Y. J. Phys. Chem. B 2011, 115, 5678-5684.
- (82) Kleinekathöfer, U. J. Chem. Phys. 2004, 121, 2505.
- (83) Schröder, M.; Schreiber, M.; Kleinekathöfer, U. J. Chem. Phys. **2007**, 126, 114102.
- (84) Ishizaki, A.; Fleming, G. R. J. Chem. Phys. 2009, 130, 234110-8.
- (85) Chen, X.; Silbey, R. J. J. Phys. Chem. B 2011, 115, 5499-5509.
- (86) Hein, B.; Kreisbeck, C.; Kramer, T.; Rodríguez, M. New J. Phys. **2012**, 14, 023018.
- (87) Tian, B.; Ding, J.; Xu, R.; Yan, Y. J. Chem. Phys. 2010, 133, 114112.
- (88) Hu, J.; Xu, R.; Yan, Y. J. Chem. Phys. 2010, 133, 101106.
- (89) Tanimura, Y.; Mukamel, S. J. Phys. Soc. Jpn. 1994, 63, 66-77.
- (90) Tanaka, M.; Tanimura, Y. J. Phys. Soc. Jpn. 2009, 78, 73802.
  (91) Tanaka, M.; Tanimura, Y. J. Chem. Phys. 2010, 132, 214502.
- (92) Meier, C.; Tannor, D. J. Chem. Phys. 1999, 111, 3365.
- (93) Tanimura, Y.; Wolynes, P. Phys. Rev. A 1991, 43, 4131–4142.
- (94) Fehlberg, E. Computing **1985**, 34, 265–270.
- (95) Hu, X.; Schulten, K. Biophys. J. 1998, 75, 683-694.
- (96) Sakurai, A.; Tanimura, Y. J. Phys. Chem. A 2011, 115, 4009-4022.
- (97) Dijkstra, A.; Tanimura, Y. New J. Phys. 2010, 12, 055005.
- (98) Xu, D.; Schulten, K. Chem. Phys. 1994, 182, 91-117.
- (99) Palma, G. M.; Suominen, K.-A.; Ekert, A. K. *Proc. R. Soc. A* **1996**, 452, 567–584.
- (100) Stamp, P.; Gaita-Ariño, A. J. Mater. Chem. 2009, 19, 1718-1730.
- (101) Caruso, F.; Huelga, S. F.; Plenio, M. B. Phys. Rev. Lett. 2010, 105, 190501.